Spectral components of detergent-solubilized bovine cytochrome oxidase

Mariana C. Rocha, Roger Springett

PII: S0005-2728(18)30083-5
DOI: doi:10.1016/j.bbabio.2018.04.009
Reference: BBABIO 47908

To appear in:

Received date: 5 October 2017
Revised date: 21 March 2018
Accepted date: 23 April 2018

Please cite this article as: Mariana C. Rocha, Roger Springett , Spectral components of detergent-solubilized bovine cytochrome oxidase. The address for the corresponding author was captured as affiliation for all authors. Please check if appropriate. Bbabio(2018), doi:10.1016/j.bbabio.2018.04.009

Spectral components of detergent-solubilized bovine cytochrome oxidase

Mariana C. Rocha[2] and Roger Springett[1*]

[1]Medical Research Council Mitochondrial Biology Unit, University of Cambridge, Cambridge Biomedical Campus, Wellcome Trust/MRC Building, Hills Road, Cambridge, CB2 0XY, UK, [2]Cardiovascular Division, King's College London, British Heart Foundation Centre of Excellence, 125 Coldharbour Lane, London SE5 9NU, United Kingdom.

[*]Current address: Cardiovascular Division, King's College London, British Heart Foundation Centre of Excellence, 125 Coldharbour Lane, London SE5 9NU, United Kingdom.

Running title: Spectral components of CytOx

Address all correspondence to Roger Springett at:

e-mail: Roger.Springett@kcl.ac.uk

Highlights

- Redox titrations were performed on the isolated detergent-solubilized bovine enzyme
- The Soret- and α-band was analyzed with precise multiwavelength spectroscopy
- The presence of the 602nm form of heme *a* was verified
- This state was stabilized at high pH and on binding of azide
- Results confirm that redox titrations can be successfully performed in living cells

Keywords Cytochrome oxidase, midpoint potential, proton pumping, heme spectroscopy, redox titration, azide.

Abstract

Cytochrome oxidase is the terminal oxidase of the mitochondrial electron transport chain and pumps 4 protons per oxygen reduced to water. Spectral shifts in the α-band of heme *a* have been observed in multiple studies and these shifts have the potential to shed light on the proton pumping intermediates. Previously we found that heme *a* had two spectral components in the α-band during redox titrations in living RAW 264.7 mouse macrophage cells, the classical 605nm form and a blue-shifted 602nm form. To confirm these spectral changes were not an artifact due to the complex milieu of the living cell, redox titrations were performed in the isolated detergent-solubilized bovine enzyme from both the Soret- and α-band using precise multiwavelength spectroscopy. This data verified the presence of the 602nm form in the α-band, revealed a similar shift of heme *a* in the Soret-band and ruled out the reversal of calcium binding as the origin of the blue shift. The 602nm form was found to be stabilized at high pH or by binding of azide, which is known to blue shift the α-band of heme *a*. Azide also stabilized the 602nm form in the living cells. It is concluded there is a form of cytochrome oxidase in which heme *a* undergoes a blue shift to a 602nm form and that redox titrations can be successfully performed in living cells where the oxidase operates in its authentic environment and in the presence of a proton motive force.

1. Introduction

Cytochrome oxidase is the terminal oxidase of the mitochondrial electron transport chain which pumps 4 protons per oxygen reduced [1]. Electrons from intermembrane cytochrome *c* (Cyt*c*) are first passed to the Cu_A centre located on the cytosolic side of the enzyme and subsequently to heme *a*, located at a depth of approximately 1/3 of the membrane thickness [2-3]. Electrons are then passed parallel to the membrane to the binuclear centre (BNC) consisting of heme a_3 and Cu_B, where oxygen is reduced to water. The catalytic cycle has been well documented [4]. Oxygen binds to the binuclear centre when both heme a_3 and Cu_B are reduced (R-state) to form the A-state, and is reduced in a concerted 4-electron transfer [5] to form the P-state with a ΔG that makes this reaction essentially irreversible [6]. Two electrons are derived from heme a_3, one from Cu_B and one from a nearby tyrosine. The BNC and the tyrosine are then re-reduced by 4 sequential electron transfers from heme *a* forming the F, O, E and R state but, in the low dielectric constant of the protein, each electron must be accompanied by a substrate proton for charge neutralization [7]. These substrate protons combine with the charged oxygen intermediates ligated to the BNC to form water.

Proton pumping is initiated by reduction of heme *a* which raises the pK_a of a pump loading site (PLS) above the hemes allowing it to be protonated from the N-side [8]. Prior to protonation, the midpoint potential (E_m) of heme a_3 and Cu_B is far below heme *a* so that the equilibrium prevents the BNC from becoming reduced. Protonation of the PLS raises the midpoint potential of the BNC which changes the equilibrium allowing substantial electron transfer to the BNC. Subsequent uptake of the substrate proton neutralizes the charge at the binuclear centre, lowers the pK_a of the PLS and ejects the pump proton to the P-side. The precise details of the pumping mechanism are still poorly understood. Much of the information on the catalytic cycle and proton pumping has been gained using dual-wavelength difference spectroscopy of the hemes. However this analysis neglects the small spectral shifts in the α-band that have been observed in redox titrations [9-11], after CO photolysis in the mixed valence enzyme [12], after photo injection of an electron in the Cu_A site [8] and stopped-flow mixing with reduced Cyt*c* [13]. These spectral changes have the potential to shed more light on the nature of the proton pumping intermediates.

Both heme *a* and a_3 have similar midpoint potentials and strongly overlapping absorption spectra in the α- and Soret-band making the separation of their spectra problematic. The classical approach has been to first lock heme a_3 fully oxidized with cyanide and then measure the difference spectrum of heme *a* [14]. The difference spectrum of heme a_3 is then calculated by subtracting the heme *a* spectrum from the fully reduced-oxidized spectrum of the unligated enzyme. This revealed that the difference spectra of heme *a* and a_3 in the Soret-band have nearly equal strength with peaks at 446 and 444nm, respectively, whereas the α-band is dominated by heme *a* with a peak at 605nm while the spectrum of heme a_3 is much broader and weaker [14]. The use of other ligands, including carbon monoxide, which locks heme a_3 in the reduced form, provides very similar spectral shape and intensity for heme *a* confirming this assignment [15-16]. Early redox titrations, which probe intermediate levels of reduction, in both isolated mitochondria [17] and the detergent-solubilized enzyme [11], indicated that there were two bands of similar width to the classical spectrum of heme *a* but with equal intensity, and both components titrated with an n=1 Nernst function. One band had a peak at ≈603nm and a high midpoint potential whereas the other had a peak at ≈607 and a low midpoint potential. These were inevitably assigned to heme *a* and a_3, respectively, in sharp contrast to the classical spectra. The discrepancy was partially resolved when it was determined that considerable redox anti-cooperativity existed between the hemes [18], such that both have a high midpoint potential (≈340mV) when the other heme is oxidized, and there was a strong interaction of ≈100mV, consistent with Coulomb repulsion [19], which gives them a low midpoint potential (≈240mV) when the other heme is reduced. However, the origin of the spectral shift observed during the titrations was not resolved and was left as: "the difference spectrum peaks at wavelengths just below 605 nm for the oxidized to half-reduced transition, but just above 605 nm for the half reduced to reduced transition of the enzyme" [20].

More recently, we found that the spectrum of heme *a* in living RAW 264.7 mouse macrophage cells had a peak at 602nm in the presence of a proton motive force, but shifted to the classic 605nm form when the proton motive force was collapsed with a proton ionophore [21]. This data allowed us to extract an absorption spectrum which had nearly equal width and magnitude as the classic 605nm spectrum but a peak at 602nm. When this spectrum was used in combination with the classical heme *a* spectrum to analyze attenuation spectra from redox titrations of CytOx in the living cells, we found that the 602nm form titrated as heme *a* when heme a_3 is oxidized and the 605nm form titrated as heme *a* when heme a_3 is reduced. This model was able to explain the spectral shifts observed previously was compatible with the anti-cooperativity between the hemes and used the classical heme spectra, albeit with an additional form of heme *a* blue shifted to 602nm. However, the line width of these features precludes their spectral resolution and they can only be separated with multiwavelength fitting requiring more precise spectroscopic measurements than needed for dual-wavelength difference spectroscopy. These results were met with considerable skepticism, at least partly due to the complex milieu of the living cell, citing the peak shift of heme *a* with Ca^{2+} binding [22-24] (see [25] for a recent review) and with pH [26], and interference from the 607nm feature of the BNC in the F and P_R state [27] due to the use of oxygen as an oxidant during the titrations. Here we perform precise and simultaneous spectroscopic measurements from the Soret- and α-band of isolated detergent-solubilized bovine cytochrome oxidase to address these criticisms and shed more light on the origin of the two forms of heme *a*.

2. Materials and Methods

2.1 Spectroscopy

Attenuation measurements were made in a custom chamber containing a 2mL cuvette with a 1cm pathlength. The cuvette has mounted in an aluminum block and held at 37±0.01°C with an Arroyo Instruments 5305 5A/12V TEC Source using an AD590 temperature transducer mounted in the block and two 6W thermoelectric elements mounted under the block.

Light from a 3-phosphor LED was coupled into a 1.0mm optic fiber with NA 0.37 and collimated with a 7.86mm focal length aspheric collimator lens with NA 0.51. The collimated beam passed through the cuvette and into a 19mm Teflon integrating sphere built into the aluminum block. Light from the integrating sphere was collected with two 1mm NA0.37 optic fibers and F# matched onto two F4.1 0.32m spectrographs each equipped with 600g/mm gratings and a 1024x128 pixel CCD cooled to 214K. One spectrograph was tuned to give spectra from 508-640nm (α-band) and the other from 390-580nm (Soret-band) with a 0.13nm pixel band pass. The slits were set to give a 1nm spectral resolution. The dispersion across the CCDs was determined from the grating equation using the spectrograph's centre wavelength, the focal length of the spectrograph's output mirror and the tilt of the CCD with respect to the focal plane. These 3 parameters were calibrated for each spectrograph using >20 lines of a low pressure neon lamp and then, daily, the center wavelength was calibrated with the 546, 573 and 576nm lines (α-band) or the 435nm line (Soret-band) of a low pressure mercury lamp. The position of the calibration lines was determined with sub pixel accuracy from the maximum of a quadratic function fitted to the center pixel of the peak and one pixel each side of the peak. The calibration accuracy was <0.01nm and the spectrograph grating was not rotated between calibration and measurement precluding mechanical error; the day to day drift in the calibration was <0.02nm.

2.2 CytOx preparation

Mitochondria were isolated from bovine hearts [28] then mitochondrial membranes were prepared by disruption with a Waring blender in the presence of KCl [29]. The final pellet was resuspended in 20 mM Tris-HCl (pH 7.4) with 10% v/v glycerol and 1 mM EDTA and 10mL aliquots were stored at −80°C. Aliquots were thawed slowly on ice and then solubilized with 1% n-dodecyl-β-D-maltoside (DDM, Anatrace), stirred for 20 min, and then centrifuged for 23 min at 34500g. The

supernatant was filtered and then applied to a pre-equilibrated 16 mL Q-Sepharose HP column (Amersham Pharmacia Biotech). Buffer A for the elution contained 20 mM Tris-HCl (pH 7.4), 10% (v/v) ethylene glycol, 0.1% (w/v) DDM and 0.005% (w/v) phenylmethanesulfonyl fluoride(PMSF), and buffer B contained 1M NaCl. The Q-Sepharose column was washed with 16 mL of buffer A and then CytOx was eluted as a green fraction at ≈250mM by a linear gradient to 350mM NaCl (30 mL at 2mL min^{-1}). The green fractions were pooled, concentrated with a 100 kDa Amicon Ultra-15 centrifugal filter unit to a concentration of 60-80μM, and then frozen at −20°C until use. This fraction was soluble in aqueous buffers with no additional detergent.

2.3 Equilibrium model

The data was analyzed in terms of an equilibrium Markov state model [30-31] rather than an equilibrium redox model (see appendix of [32]). Both models produce precisely the same results when applied to the same system but the former is used because (1) it is a more fundamental description of the system as it is based on equilibrium statistical thermodynamics, (2) it is more appropriate when a redox centre can be split into multiple states based on spectroscopy and (3) so that these states can be used in an *in-silico* Markov state model of turnover at a later time. The states, σ, were described as <X,n_H,n_L> where X is the redox state of heme *a* and a_3, n_H is the number of protons bound and n_L is the number of ligands, L, bound. Only azide was considered as a ligand in this study. Five redox states were included in the model: the enzyme with both hemes oxidized (*o*), with only heme *a* reduced having a peak at 605nm (a_{605}) or at 602nm (a_{602}), with only heme a_3 reduced (a_3) and with both hemes reduced (aa_3). The energy of a state, E^σ, is given by

	$E^\sigma = E_0^\sigma + n_e E_h - n_H k_B T \,\mathrm{Ln}([H^+]) - n_L k_B T \,\mathrm{Ln}([L])$	Equation 1

Where E_0^σ is the energy of the state under standard conditions, E_h is the ambient redox potential, n_e is the number of electrons of the state (0 for *o*, 1 for a_{605}, a_{602} and a_3, and 2 for aa_3) k_B is Boltzmann's constant, *T* is the absolute temperature in Kelvin and the square brackets denote the concentration of the species divided by the concentration of the species under standard conditions. The probability of an individual CytOx protein being in state σ, P^σ, is determined by the Boltzmann distribution and given by

	$P^\sigma = \dfrac{e^{-E^\sigma/k_B T}}{\sum_\sigma e^{-E^\sigma/k_B T}}$	Equation 2

Where the denominator is the partition function which is the sum is over all states. The standard potential of the unligated oxidized state was set to zero. The attenuation spectrum, $A(\lambda)$, of a cuvette with pathlength *d* and CytOx in a distribution of states with total concentration *C* is given by:

	$A(\lambda) = dC\sum_\sigma P^\sigma \varepsilon_\sigma(\lambda)$	Equation 3

where $\varepsilon_\sigma(\lambda)$ is the specific extinction spectrum of the σ state and assumed to be the sum of the contributions from heme *a* and a_3.

Where a spectroscopic signal can be attributed to multiple states, the signal is proportional to the sum of the probabilities of each state and an effective energy can be defined as

	$E^s = -k_B T \,\mathrm{Ln}\left(\sum_\sigma e^{-E^\sigma/k_B T}\right)$	Equation 4

where the sum is over all the states forming the spectroscopic signal.

The midpoint potential for a redox couple from an oxidized state (*O*) to a reduced state (*R*), $E_m^{O\to R}$, is given by:

	$E_m^{O\to R} = E_0^O - E_0^R$	Equation 5

where E_0^O and E_0^R are the standard energies of the oxidized and reduced form, respectively. The K_d for ligand binding from an unbound state (U) to a bound state (B) is given by:

	$k_B T \,\mathrm{Ln}\left(K_d^{U\to B}\right) = E_0^B - E_0^U$	Equation 6

Where E_0^U and E_0^B are the standard energies of the unbound and bound form, respectively.

Standard conditions are defined here as: 37°C, pH 7.0, azide 1M. Potentials are expressed in millivolts (mV), where 10.46mV=1KJ/mole, so that the model can be directly compared to the membrane potential and redox potentials of the substrates in the future. In mV, k_BT = 26.7mV and k_BT Ln(10) = 61.5mV.

2.4 Redox titrations of detergent solubilized bovine CytOx

Redox titrations were carried out in a 100mM potassium phosphate / potassium hydroxide buffer at pHs between 6.0 and 9.0 with 200μM BAPTA to chelate out any calcium ions. At pH 9.0, 100mM phosphate still has a buffering capacity of 3.62mM/pH unit but the actual pH of the buffer was measured at the end of the study with a pH electrode. High free calcium was obtained by addition of 250μM of $CaSO_4$. NADH was used as a reductant and 10μM phenazine ethosulfate (PES) as a redox mediator. Titrations were carried out using either oxygen as an oxidant or the FIRE protocol as a reductant [32] and the ambient redox potential was monitored from the oxidation state of Cyt*c* assuming a midpoint potential of 260mV; the titration analysis was restricted to the range 2-98% oxidized (260±104mV).

The 2mL cuvette was sealed from the top with a stainless steel plunger through which a length of fine gauge silicone tubing (OD 0.94mm, ID 0.51mm, Helix Medical Europe) was threaded such that it formed a 15mm loop within the cuvette. A computerized gas blender generated a nitrogen /oxygen gas mixture which was passed through the tubing allowing oxygen to diffuse into the cuvette at a rate depending on the difference in oxygen tension across the wall of the tubing. The cuvette was stirred with a glass-coated magnetic bead and the tubing extended the height of the cuvette so that the oxygen that diffused through the tubing was rapidly homogenized throughout the cuvette. The oxygen concentration in the cuvette was measured using a custom made phase-flurometer from the lifetime of an oxygen-sensitive phosphorescent optode (Tau Theta, Bolder, CO) inserted through a hole in the side and sealed with a viton o-ring. The phosphorescent optode was excited with light from a filtered 385nm LED which was square wave modulated at 4KHz. The 650nm phosphorescent emission was long-pass filtered and detected with a silicon photodiode and the output digitized at 1MHz. The phase was determined from the 1st harmonic, converted to a quench rate, and the non-linearity between quench rate and oxygen concentration was calibrated against a Clarke electrode.

Initially ≈2.0μM cytochrome oxidase and ≈3.6μM of horse heart Cyt*c* (Sigma) was added to the cuvette at ambient oxygenation (≈200μM) and then CytOx turnover was initiated by adding 500μM of NADH. Once the cuvette became anoxic, the excess NADH was then consumed by flowing 5% oxygen through the tubing until the Cyt*c* oxidized and the oxygen concentration rose to ≈1μM. The CytOx and Cyt*c* was reduced again with 25μM of NADH and then the oxygen in the tubing was increased to 2% and the Cyt*c* swept from fully reduced to fully oxidized over a period of 7-8 minutes while spectra were collected contiguously with a temporal resolution of 500ms. During the titration, CytOx immediately consumed the oxygen delivered by the tubing so that the cuvette was

maintained anoxic to within the noise floor of the oxygen optode (0.04μM) until the CytOx was almost fully oxidized (see fig. S.6 of the supplementary information). The oxygen delivery was estimated to be ≈1.5μM/minute so that the titration was performed at a CytOx turnover rate of approximately 1 oxygen every 80 seconds. This slow turnover rate should ensure that tight equilibrium with Cyt*c* was maintained throughout the titration and also that CytOx was kept in the active form. The FIRE protocol used 1μM riboflavin as photocatalyst and 2mM of EDTA as the ultimate reductant with 10μM PES as redox mediator. The riboflavin was photoexcited with a pulse of light from a 450nm high power blue LED which was time multiplexed with the white detection LED using a duty cycle of 6ms on and 4ms off and a cycle time of 20ms. The CCDs were read in the off period after every pulse and the attenuation spectrum from the white LED was average to give a temporal resolution of 500ms. This allowed attenuation spectra of CytOx to be collected continuously, and without interference from the blue LED, as the oxidation state of Cyt*c* was swept from fully oxidized to fully reduced over a period of ≈3 minutes. When a FIRE titration was carried out immediately after an oxygen titration, the data overlaid and the fitted midpoint potentials of the different states varied by <3mV (fig. S.1 of the supplementary information). This shows that the Cyt*c* and the heme *a* and a_3 of CytOx were maintained in redox equilibrium to ≈3mV during the titration and that the CytOx did not relax into a form with different redox properties on the timescale of two-titrations (≈10 minutes).

2.4 Redox Titrations of mouse CytOx in living cells

Titrations in RAW 264.7 mouse macrophages have been described previously [21]. In brief, cells were cultured in RPMI media with 10% FBS and antibiotics in a humidified 5% CO_2 incubator, then spun down at 500g for 5 minutes and resuspended at a density of 2.0×10^7 cells/mL in RPMI. Spectroscopic measurements were carried out in a custom 5mL chamber maintained at 37°C containing 80mm of silicone tubing through which a N_2:O_2:5% CO_2 gas mixture was passed. The cells were made anoxic and then the proton motive force collapsed with a combination of 5ug/mL of oligomycin and 2uM of the protonophore BAM15. The cells were then treated with 1μM of rotenone to inhibit complex I and the gas mixture in the tubing increased to 2% to initiate oxidation of the succinate/fumarate pool via complex II, complex III and complex IV. This procedure swept Cyt*c* from almost fully reduced to almost fully oxidized over a period of 2 minutes as the succinate pool was depleted. The oxygen in the tubing was then returned to 0% and the Cyt*c* re-reduced. The cells were then treated with 1mM of sodium azide and a second titration carried out by switching the oxygen in the tubing to 2%. The ambient redox potential was monitored from the oxidation state of Cyt*c* in the range 5-95% (260±79mV) assuming a midpoint potential of 260mV and data collection was every 500ms allowing the collection of ≈200 data points in the titration range of Cyt*c*.

2.5 Spectral Fitting

Attenuation spectra were fitted to a model consisting of a linear combination of the chromophores and a polynomial background, e.g.

	$\Delta A(\lambda) = \rho \sum_c \Delta C_c \varepsilon_c(\lambda) + \sum_n a_n \lambda^n$	Equation 7

Where ρ is the pathlength, ΔC_c is the change in oxidation of the c^{th} chromophore, $\varepsilon_c(\lambda)$ is the specific absorption spectrum of the c^{th} chromophore, the first sum is over all chromophores and the second sum is a polynomial background. The fitting range was 520-630nm for the α-band and 405-480nm for the Soret-band.

The reference difference (oxidized-reduced) spectra for heme a_3 and heme $a_{605/446}$ (heme *a* with a peak at 605nm and 446nm in the α- and Soret-band, respectively) was from Liao and Palmer [14] and the tabulated data downloaded from the author's website. The spectrum of heme a_{602} and a_{443} were obtained by blue shifting the heme $a_{605/446}$ spectrum by 3nm. The isolated enzyme was fitted

with the difference spectra of $a_{605/443}$, $a_{602/443}$, a_3 and horse heart Cyt*c* with a linear background. The mouse cells were fitted with the difference spectra of a_{605}, a_{602}, a_3, mouse Cyt*c*, b_H, b_L and c_1 with a quadratic background to correct for small changes in scattering coefficient of the turbid media.

The spectral component of Cyt*c* was removed from the change in attenuation spectra by subtracting $\rho \Delta C \varepsilon(\lambda)$ where ΔC is the fitted change in oxidation of Cyt*c* and $\varepsilon(\lambda)$ is the specific absorption spectrum of Cyt*c*.

2.2 Measurement of spectral shifts

From the definition of the first differential, the spectrum of a feature shifted by $\delta\lambda$ is approximated by:

	$\varepsilon(\lambda+\delta\lambda) \approx \varepsilon(\lambda) + \frac{d\varepsilon}{d\lambda}\delta\lambda$	Equation 8

Where $\varepsilon(\lambda+\delta\lambda)$ and $\varepsilon(\lambda)$ are the shifted and unshifted spectra, respectively, and $d\varepsilon/d\lambda$ is the first differential of the unshifted spectrum with respect to wavelength, λ. The spectrum of $d\varepsilon/d\lambda$ is included into the fitting model as a pseudochromophore and the effective change in concentration (ΔC_c) from the fitting is the product of the pathlength, change in concentration of heme *a* and the wavelength shift. The wavelength shift can then be calculated by dividing by the change in heme *a* concentration.

3. Results

3.1 The spectral shift in the α-band.

Figure 1 shows changes in the α-band attenuation spectrum of detergent solubilized bovine CytOx on reduction from the oxidized state at pH 8.0 when the calcium was chelated with BAPTA. The component of Cyt*c* was spectrally subtracted (see Methods) to allow a clearer view of the spectral shift of the α-band (see fig. S.2 of the supplementary information for the original spectra). The α-band peak first appears at ≈603nm, then undergoes a red shift to ≈604nm at an ambient redox potential of 200mV and finally shifts to 605nm when fully reduced (fig. 1). The inset of fig. 1 shows the spectrum at a redox potential of 280mV (when heme *a* is half reduced) minus the fully oxidized spectrum in red, which has a peak at ≈603nm, and the fully reduced spectrum minus the spectrum at 280mV (blue), which has a peak at ≈607nm. This data confirms "the difference spectrum peaks at wavelengths just below 605 nm for the oxidized to half-reduced transition, but just above 605 nm for the half reduced to reduced transition of the enzyme" [20].

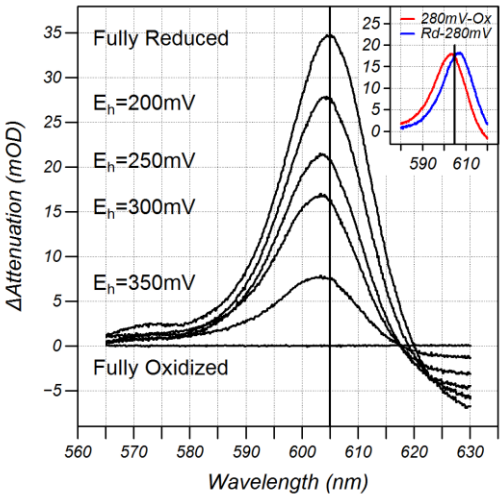

Figure 1. Changes in the α-band attenuation spectrum of CytOx on reduction from the oxidized state at pH 8.0. The black vertical lines are drawn at 605nm to emphasize the small spectral shifts. The inset shows the spectrum at a redox potential of 280mV (half reduced) minus the fully oxidized spectrum (red) and the fully reduced spectrum minus the spectrum at 280mV (blue).

To further investigate the spectral shifts, we performed titrations at different pHs in the presence and absence of calcium. The full-width at half-maximum of the heme *a* spectrum is broad (approximately 17nm) making it difficult to precisely quantify small spectral shifts directly from the spectrum. Therefore, the reference spectrum and its first differential were first fitted to the attenuation spectra and then the spectral shift relative to the reference spectrum was calculated from the relative magnitude of the two components (see methods). This technique is expected to be highly accurate for heme *a* when the peak-shift is small (<±2nm) but likely to underestimate it when the peak shift is larger. Using this technique on the attenuation spectra, we found that, when the adventitious calcium was chelated with BAPTA, the blue shift at intermediate redox potentials is greater at high pH (fig. 2, blue traces) and the peak position of the fully reduced CytOx is also pH dependent above pH ≈7.5 (fig. 2 inset). Also, this technique was sensitive enough to show that, in the fully reduced enzyme at a pH range of 6.0-7.5, where the α-band position is independent of pH, the precise position of the α-band varies by 0.2-0.5nm from the reference spectrum depending on the isolation batch (data not shown). Previously it has been demonstrated that binding of calcium to the cation binding site red-shifts the α-band of both the fully reduced enzyme [22] and cyanide-inhibited mixed valence bovine enzyme [22-24]. As shown in fig. 2, calcium binding also red shifts the heme *a* band at intermediate redox potentials (red traces), although to a lesser extent than blue shift

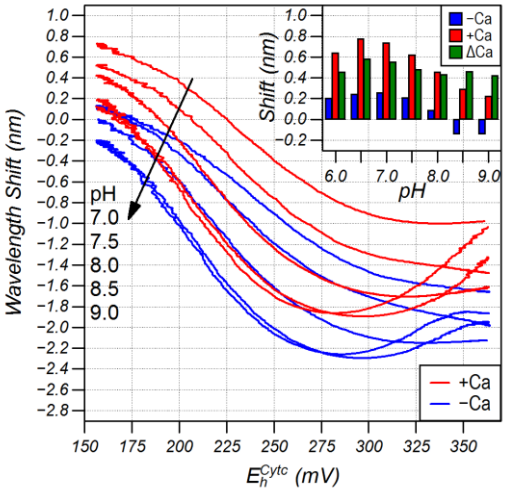

Figure 2. Wavelength shift of the α-band of heme *a* as a function of redox potential at increasing pHs (7.0, 7.5, 8.0, 8.5 and 9.0). Blue and red traces indicate the absence of calcium (chelated by 200μM BAPTA) and presence of calcium (addition of 250μM $CaSO_4$), respectively. Inset: wavelength shift when fully reduced. Green bars are the shift on calcium binding to the fully reduced enzyme.

from the reference spectrum. The α-band peak position of the Ca-bound fully-reduced enzyme remains pH dependent (fig. 2 inset) but the red-shift on calcium binding (green bars) is independent of pH (mean±SD of 0.43±0.06 nm) indicating that the red-shift with calcium is additive to the blue-shift with pH.

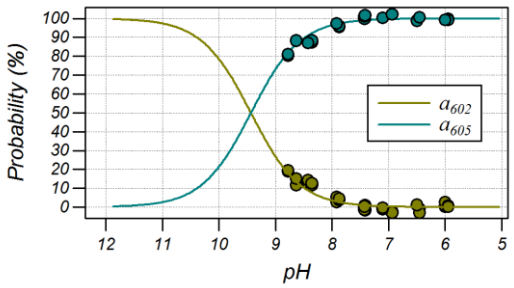

Figure 3. The fraction of the a_{605} and a_{602} spectra to the attenuation spectrum of fully reduced CytOx as a function of pH. CytOx was reduced with NADH, using PES as a redox mediator, and in the presence of 200μM BAPTA to chelate calcium. Data points are from 3 studies and the lines are from a disassociation function with a pK_a of 9.4.

3.2 Blue shift in the Fully Reduced Enzyme.

To further investigate the origin of the blue shift with pH of the fully reduced enzyme in the absence of calcium (inset of fig. 2), the difference attenuation spectra at different pHs were fitted to a spectral model that consisted of: the Cyt*c* difference spectrum, the reference heme *a* difference spectrum (a_{605}), the reference heme a_3 difference spectrum (a_3) and the reference spectrum of heme *a* blue-shifted by 3nm to have a peak at 602nm (a_{602}). It was found that, at high pH, the peak shift in the inset of fig. 2 can be attributed to an increased fraction of the 602nm form of heme *a* (fig. 3). This conversion from the 605 to the 602nm occurred with a pK_a of ≈9.4, as determined by fitting a disassociation curve to the fraction of each spectral component in the reduced spectrum (fig. 3). Usually, it is difficult to determine a pK_a if the data points do not cover the plateau above and below the pK_a [25] but it is more reliable in this case because the probability, and hence the extent of the change, is known.

3.3 Spectral components of the α-band

To explore the origin of the spectral shifts at intermediate redox potentials, the attenuation spectra from a redox titration of the detergent-solubilized bovine CytOx was fitted with the Cyt*c*, a_{605}, a_{602} and a_3 spectral components, and the signal of the heme components were plotted as a function of the redox potential of Cyt*c* (fig. 4a). While the spectral fitting algorithm could not successfully separate the heme a_3 spectral component in the mouse cells (because the absorption is weak, broad and nearly collinear with the quadratic background used to correct for small baseline offsets) this could be achieved in the cleaner spectral environment of the detergent-solubilized enzyme. The spectral components of the α-band at different redox potentials are shown in fig. S.3 of the

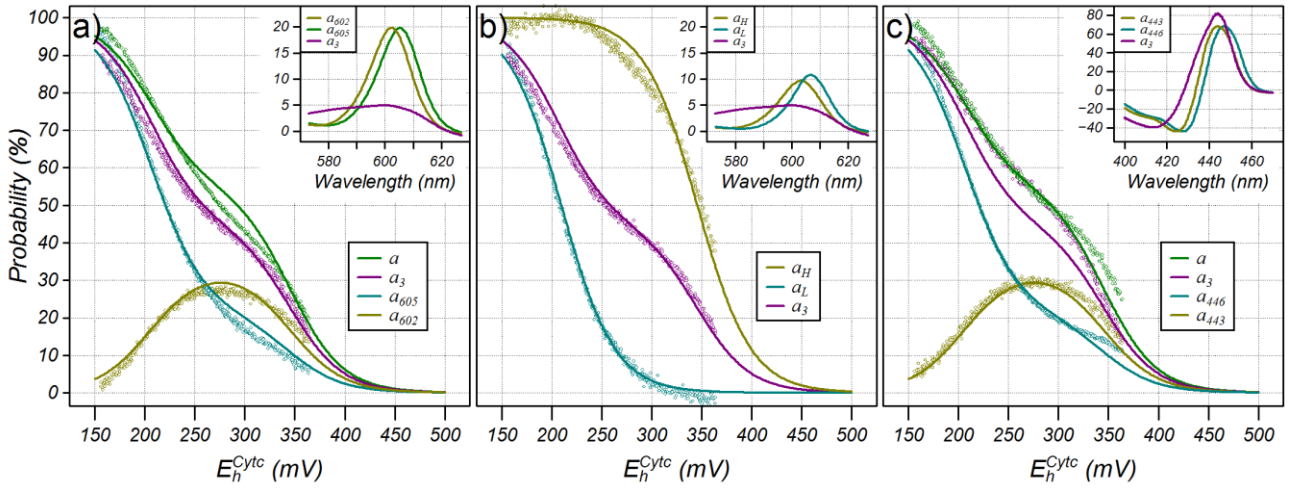

Figure 4. Redox titrations of the α-band of CytOx at pH 7.5. The experimental data is shown as points, the lines are a fit to a redox model and the spectra for the fitting model are shown in the insert. a) Titrations from the α-band using the standard a_{605} and a_3 spectra along with the a_{602} spectrum. The data was fit to a 5 state model of redox cooperativity. b) The same spectra data as a) but fitted using a linear combination of the a_{605} and a_{602} spectra which titrate as n=1 Nernst functions (lines). c) Titrations from the Soret-band using the reference spectrum of heme *a* (a_{446}) and a_3, and the reference spectrum of heme *a* blue shifted by 3nm (a_{443}). The lines are from the model in a) shown to emphasize the differences between the data obtained from the α- and Soret-bands.

supplementary information where it can be seen that the a_{605} and a_{602} components merge together to form the α-band and are never spectrally resolved. The attenuation spectrum is dominated by the 602nm form as the ambient redox potential is reduced from the oxidized state to 280mV (fig S.3) but with a small contribution from the 605nm form and a_3 such that the compound spectrum has a peak at ≈603nm (inset of fig. 1). On further reduction from 280mV to the fully reduced state, the 602nm component is lost and the spectrum becomes dominated by the 605nm component with weaker intensity from the a_3 spectrum. In this range, the loss of absorption at 602nm and the increase at 605nm together with the broad a_3 spectrum leads to a compound difference spectrum with a peak at ≈607nm (inset of fig. 1). Fig. S.4 of the supplementary information confirms that the α-band cannot be successfully fitted without the 602nm spectral component, as was previously found in the mouse cells.

The signal of each component was first compared to a standard redox model of the two hemes with anti-cooperativity. This model contained 4 states: the *o* state with both hemes oxidized, the *a* state in which only heme *a* is reduced, the a_3 state in which only heme a_3 is reduced and the aa_3 state in which both hemes are reduced. The states with only one heme reduced (*a* and a_3) in a two-center anti-cooperativity model titrate with the same bell-shape but with different magnitudes depending on the relative midpoint potential whereas the state with both hemes reduced (aa_3) titrates with a shape similar to an n=1 Nernst function (fig. S.5 of the supplementary information). As in the case of redox titrations in living RAW 264.7 mouse macrophages treated with oligomycin and CCCP to collapse the proton motive force, the signal from the a_{602} spectral component has a bell-shape very similar to the a and a_3 states of the redox model and the signal from the a_{605} spectral component has a shape similar to an n=1 Nernst function (fig 4a). However, the model could not achieve a good fit to the data because the a_{605} signal had greater probability at redox potentials near the peak of the bell curve where only one heme is reduced than would be predicted if it only originated from the aa_3 state (fig S.5 of the supplementary information and the analysis therein). Therefore the *a*-state of the four state model was split into two states, one with the a_{605} spectrum and one with the a_{602} spectrum. This redox model consisted of 5 states: an *o* state with both hemes oxidized, an a_{605} state with only heme *a* reduced having the a_{605} spectrum, an a_{602} state with only heme *a* reduced but having the a_{602} spectrum, an a_3 state with only heme a_3 reduced and the aa_3-state with both hemes reduced; the a_{605} state was not needed previously in the redox model of the mouse cells to obtain a good fit. The a_{605} signal was assumed to arise from the a_{605} and aa_3 states, the a_{602} signal from the a_{602} state and the a_3 signal from the a_3 and aa_3 states. The heme *a* signal is the sum of the a_{605} and a_{602} signals. The resultant model provided a good fit to the data (fig. 4a) with both heme *a* (effective midpoint potential of the a_{602} and a_{605} states calculated with equation 4) and a_3 titrating with midpoint potentials of 330mV when the other heme is oxidized and 225mV when the other heme is reduced at pH 7.5, in good agreement with the values of 340 and 240mV obtained from previous magnetic circular dichroism studies [33] at pH 7.4. It should be noted that this redox model could account for the signal from both heme *a* and a_3 and that there are no invisible components in the model.

At any instant an individual CytOx complex is in a single state (e.g. heme *a* is either oxidized or reduced but cannot be half reduced). However, the cuvette contains many individual CytOx complexes and therefore the number of CytOx complexes in each state is determined by a probability distribution (equation 2). The attenuation spectrum of the cuvette is expected to be the algebraic sum of the absorption spectra of the individual CytOx complexes in the cuvette - and so will be the algebraic sum of the spectrum of each state weighted by the probability of finding CytOx in each state (equation 3). For example, the spectral model used to generate fig. 4a shows that 27% of the CytOx have heme *a* reduced with the a_{602} spectrum, 33% have heme *a* reduced with the a_{605} spectrum and 53% have heme a_3 reduced at an ambient redox potential of 250mV at pH 7.5. Similar to fig. S.3 of the supplementary information, the resulting attenuation spectrum has a peak at 603.6nm. The redox model shows that 27% of the CytOx are in the a_{602} state, 17% are in the a_{605} state, 37% are in the a_3 state and 16% are in the aa_3 state.

Due to the nature of linear algebra, when a spectrum can be well-fitted with one set of basis spectra then it can be equally well-fitted with any linear combination of the basis spectra. Furthermore, in a two-center redox model with strong anti-cooperativity, the aa_3 state titrates with a shape very similar to an n=1 Nernst function with a midpoint potential 19mV below the midpoint potential for the second electron in an anti-cooperativity model, as does the sum of the aa_3, a_3 and a states with a midpoint potential 19mV higher than that for the first electron (see Titration functions and basis spectra of the supplementary information). Thus, by carefully choosing two linear combinations of the a_{602} and a_{605} spectra to form two new basis spectra, it was possible to fit the attenuation spectra such that the resultant signals from the two new basis spectra follow the aa_3 state and the sum of the aa_3, a_3, and a states and both titrate as n=1 Nernst functions. For the conditions of figure 4a, the new basis spectra are approximately half the a_{602} spectrum and the a_{605} spectrum minus half the a_{602} spectrum. Both spectra are approximately half the magnitude of a_{605} spectrum (inset of fig. 4b) and have peaks at ≈602 and ≈607nm, respectively. When these spectra are used to fit the same data as in figure 4a, the signals titrate as n=1 Nernst functions with midpoint potentials of 350 and 210mV, respectively, as predicted.

Importantly, spectral shifts of heme *a* were also observed in the Soret band and, to a lesser extent in heme a_3. The technique of using the differential of the absorption spectra to quantify spectral shifts could not be used because the spectra of heme *a* and a_3 are too similar. Instead, the reference heme *a* spectrum was blue shifted to give the Soret equivalent of the a_{602} spectrum. The shift in the energy of the α-band optical transition is 82 wavenumbers and this would equate to a shift of 1.64nm at 446nm. However, the shift which gave the best correspondence between the α-band and the Soret band was found by trial and error to be ≈3nm, almost twice the shift in energy (152 wavenumbers). This difference in energy could be because the Soret- and α-band transitions originate from different unoccupied molecular orbitals .When this ad hoc spectrum (a_{443}) was used with the a_{446} , the a_3 and the Cyt*c* spectrum to fit the Soret data, the a_{446} and a_{443} components titrated in close correspondence with the a_{605} and a_{602}, respectively, at pH 7.5 (fig 4c), and there was good agreement between the Soret and α-band heme a_3 components, confirming that the spectral shift is a property of heme *a* and not an artifact of the α-band spectroscopy. This good correspondence was maintained at pH8.0 and below but was poorer at pH 8.5 and 9.0 (fig. S7 of the supplementary information).

3.4 pH Titrations

Previously we suggested that the a_{602} form is generated on the uptake of the pumped proton [21] and so, to further investigate this, redox titrations were carried out in the pH range 6.0-9.0 to separate the protonated and unprotonated forms. The titration at each pH could either be fitted with 5 redox states (*o*, a_{602}, a_{605}, a_3 and aa_3) to give effective midpoint potentials at each pH, or all the titrations could be fitted simultaneously to a model which included the 5 redox states, each with 1 or more protonation sites. The 5(N+1) standard energies, where N is the number of protonation sites, were varied using a Levenberg Marquardt algorithm [34] until the least square difference was minimized between the predicted and measured probabilities of the a_{602}, a_{605}, *a* and a_3 spectral

State	E_0 ($0H^+$)	E_0 ($1H^+$)	E_0 ($2H^+$)	pK_a 0→1	pK_a 1→2
o	0	-33.2±7.8	68.8±18.6	7.54±0.13	5.34±0.43
a_{602}	-317.5±1.1	-344.6±4.3	-297.1±4.7	7.44±0.09	6.23±0.03
a_{605}	-235.9±16.5	-349.0±4.4	-275.6±4.4	8.84±0.34	5.81±0.11
a_3	-236.4±8.6	-370.3±4.8	-286.1±9.9	9.18±0.07	5.63±0.08
aa_3	-510.2±2.6	-596.0±3.7	-536.1±6.4	8.39±0.10	6.03±0.05

Table 1 Standard energies for unprotonated, singly protonated and double protonated states, and pK_as for the model of fig. 4. Values are expressed as mean±SD (n=3 sets of titrations with each set having 7 pHs).

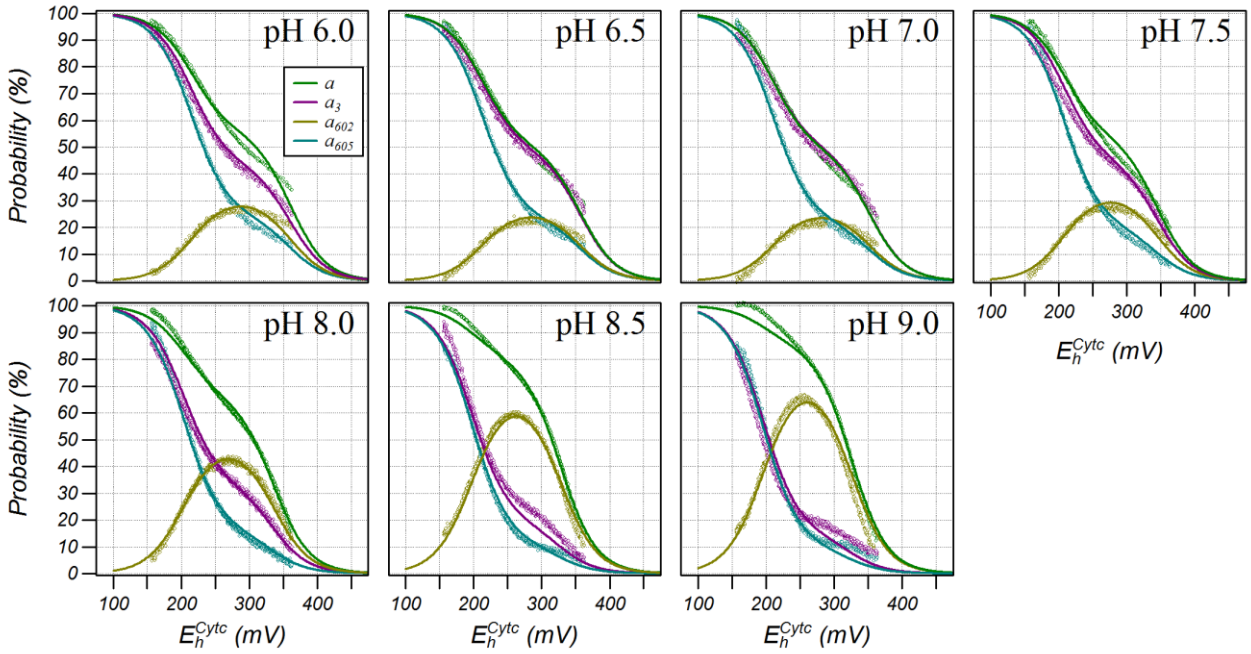

Figure 5. Redox titrations of the α-band of CytOx at increasing pH (6.0 to 9.0). The experimental data is displayed as points and the lines are a fit to a 15-state (*o*, a_{602}, a_{605}, a_3 and aa_3 with 0, 1 or 2 bound protons) model with the standard energies fitted simultaneously to all the data points.

components at all pHs. Whereas a reasonable fit was obtained with one protonation site, there were some small inaccuracies at low pH (data not shown) and a much better fit could be obtained with two protonation sites (fig. 5). These two protonation sites are in addition to the site with a pK_a of 9.4 that blue-shifts the fully reduced enzyme. That site was not included in the model of the redox titrations because it is only apparent at high pH, and at redox potentials that are too low to be quantified from the oxidation state of Cyt*c*. The standard energies and pK_a of the two binding sites are given in table 1 and the pH dependence of the standard energies of the redox states for the data in fig. 5 are shown in fig. 6a.

The predicted pH-dependent midpoint potentials calculated from the standard energies for the 4 redox couples are shown as lines in fig. 6b and compare well with the midpoint potentials when the data from each pH titration was fitted to a 5 state model separately (circles). The midpoint potentials of heme a_3 and heme *a* when it has a peak at 605nm (states a_3 and a_{605}, respectively) are strongly pH dependent for the first electron. In contrast heme *a* with a peak at 602nm for the first electron (state a_{602}), and heme *a* for the second electron (state aa_3), which has a peak at 605nm, is only weakly pH dependent.

Fig 6c shows the numbers of protons bound to each state as a function of pH. In the pH range from 7.0 to 8.0, reduction of the oxidized state to the a_{602} state does not increase the total number of protons bound, however, reduction to the a_{605} state takes up between 0.2 and 0.6 protons depending on the pH. The a_3 state can only be

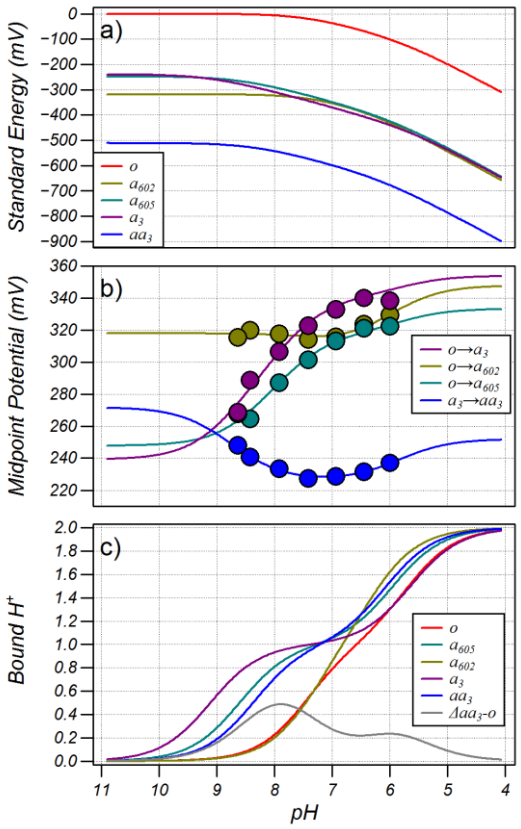

Figure 6. pH dependence of a) the standard energies, b) midpoint potentials and c) number of bound protons of the 15-state model fitted to the data of fig. 5. The data points in b) are the midpoint potentials of a 5 state model fitted individually to the data at each pH.

populated when protonated in this pH range, presumably at the BNC. Surprisingly, entry of the second electron to the a_3 state to form the aa_3 state is accompanied by the release of protons, even though the net charge on heme *a* and a_3 has become more negative. Also shown in fig. 6c is the difference in the numbers of protons bound between the fully reduced enzyme (aa_3) and the oxidized enzyme (*o*) estimating that ≈0.4 protons are taken up on full reduction in the pH range 7.5-8.0.

3.5 Redox titrations in the presence of Azide

Azide induces a blue-shift in the α-band of CytOx during turnover which is reversed when the enzyme becomes anoxic [35]. This blue-shifted spectrum is similar to a_{602} prompting us to examine the effect of azide binding on redox titrations. These titrations were carried out with the FIRE protocol as azide binds at the BNC and inhibits the reduction of oxygen. As shown in fig. 7, azide stabilizes the a_{602} state and drives the aa_3 transition to lower redox potentials, similar to the effect of high pH.

Attempts to fit the 5 states with one ligand binding site to this data consistently resulted in extremely high K_d of the ligated a_{605}, a_3 and aa_3 states, meaning that the azide did not bind at the concentrations used. The redox model with the remaining 7 states (unligated *o*, a_{602}, a_{605}, a_3 and aa_3, and single ligated, *o* and a_{602}) gave a K_d of 910μM and 670μM to the o and a_{602} states, respectively, but did not result in a good fit to the data, particularly at low azide concentrations (data not shown). Therefore a second ligand binding site was added to the model which provided the fits shown in fig. 7. This model consisted of 12 states: unligated and single ligated *o*, a_{602}, a_{605}, a_3 and aa_3 and double ligated *o* and a_{602}. The K_d for binding of the first azide to o, a_{602}, a_{605}, a_3 and aa_3 was ≈80, 90, 390, 3600 and 910μM, respectively, and the K_d for binding the second azide to *o* and a_{602} was ≈10.0 and 6.6mM, respectively. Fig. 8 compares the concentration-dependent midpoint

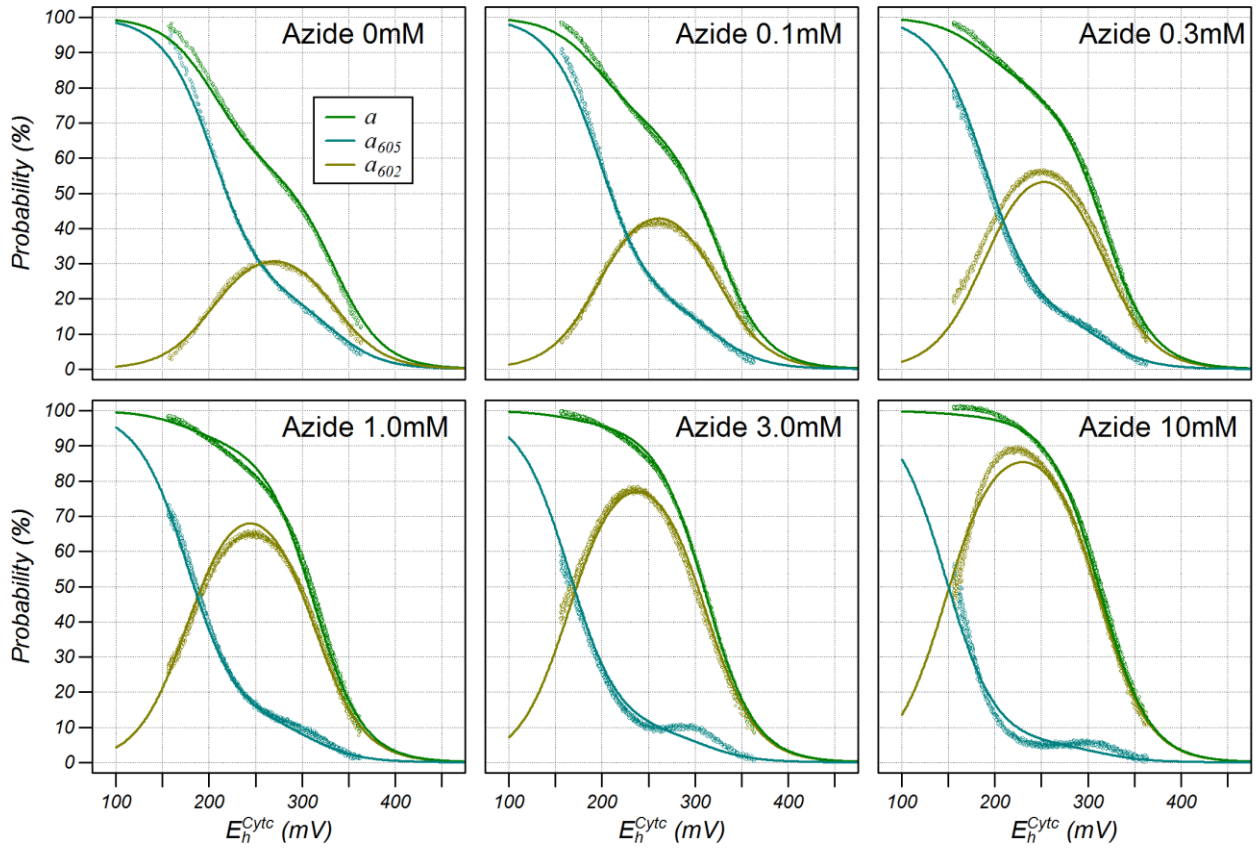

Figure 7. Redox titrations of the α-band of CytOx at increasing concentrations of sodium azide (pH 8.0). The points are the data and the lines are from a simultaneous fit to a redox model which consisted of unligated and singly ligated *o*, a_{602}, a_{605}, a_3 and aa_3, and doubly ligated *o* and a_{602}.

E_m	+FCCP	−Azide	+Azide
o→a_{602}	329.9±4.3	325.4±3.0	333.3±2.4
o→a_{605}	251.2±19	297.6 ±2.2	<230
o→a_3	292.9±2.9	315.7±7.3	283.0±6.1
a_3→aa_3	223.9±7.9	243.9±3.2	243.3±5.9

Table 2. Midpoint potentials (E_m) for a 5 state redox model to redox titrations carried out in RAW 264.7 mouse macrophages in the presence or absence of 1mM azide. +FCCP reanalysis of the FCCP treated data from [21] in the absence of azide. Values are presented as mean±SD (n=6, 4 and 4, respectively)

potentials calculated from this 12-state model (solid lines) to the midpoint potentials calculated from a 5-state model fitted to the titration data at each concentration (triangles). The dotted lines are the predicted midpoint potentials of the 12 state model but if only the first binding site is considered and shows that the midpoint potentials of the azide-bound and -unbound redox couples for the first azide binding are remarkable similar to those of the protonated and unprotonated redox couples for the first proton (table a and fig 6b).

3.6 Redox titrations from CytOx in living RAW 264.7 mouse macrophages

To determine if azide had the same effect to stabilize the a_{602} state in mouse cells, redox titrations were carried in the absence or presence of 1mM azide. These titrations were performed with the same methodology, using oxygen as an oxidant under anoxic conditions, but the proton motive force was first collapsed with a combination of oligomycin and a protonophore. The turnover number of CytOx was approximately 1.1±0.3 O_2/CytOx/s (mean±SD n=4) during the titrations. The signal to noise was poorer in mouse cells, mainly because only 50nM of CytOx is present as opposed to the 2µM in the isolated enzyme preparations, but otherwise the data was similar: the azide stabilizes the a_{602} state and drives the transition of the aa_3 state to a lower redox potential. The midpoint potentials for these titrations are given in table 2 and compared to the midpoint potentials from the bovine enzyme in fig. 8.

4. Discussion

4.1 Spectra shifts

Spectral shifts in the α-band are a common observation but the most studied effect has been observed with calcium [22, 25-26] which binds reversibly in the bovine enzyme at a specific site in subunit I on the cytosolic side of the enzyme [23]. Binding red-shifts the heme *a*

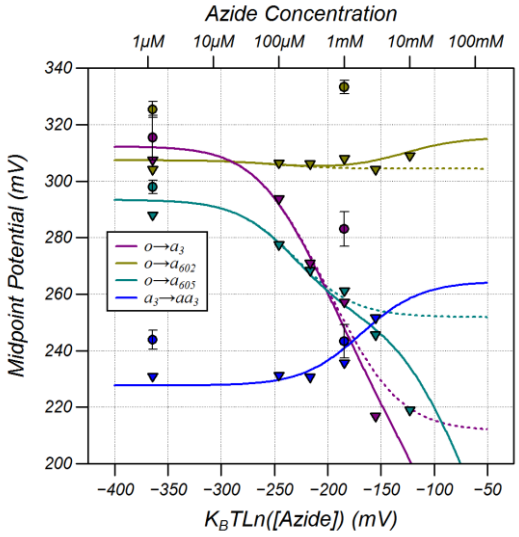

Figure 8. Effective midpoint potentials in the presence of azide. The solid lines are the predicted midpoint potentials from the redox model with both binding sites and the dotted lines are the midpoint potentials for only the high affinity site. The triangles are the midpoint potentials of a 5 state model fitted individually to the data at each pH. The circles are the midpoint potentials from the mouse cells.

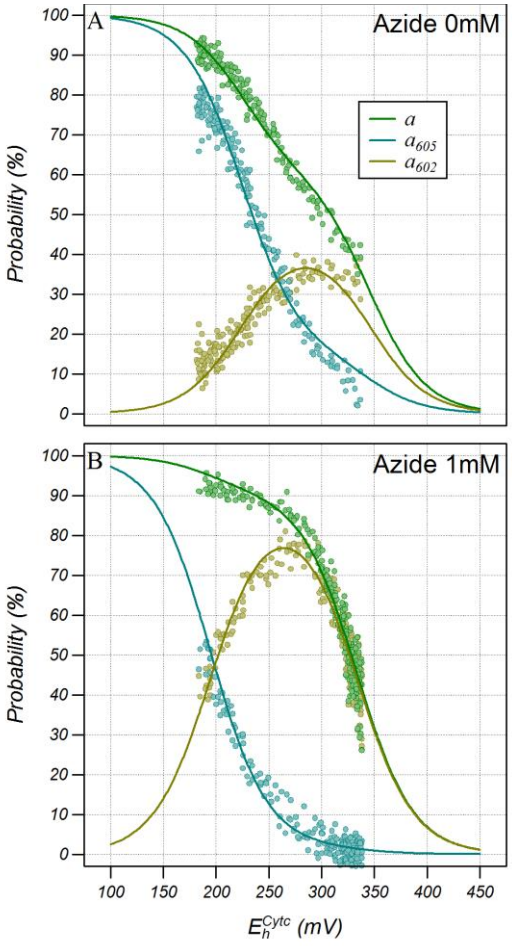

Figure 9. Redox titrations of the α-band of CytOx from living RAW 264.7 macrophages in the absence and presence of 1mM of sodium azide.

spectrum and produces a characteristic difference spectrum that can easily be used to quantify the K_d (≈3μM in a 100mM KCl buffer [25]). A shift of 0.54nm has been calculated in the Soret-band [36] but, as far as we are aware, the magnitude of the spectral shift has not been previously quantified in the α-band [22-26]. We find that the red shift is ≈0.4nm in the α-band and so reversal of calcium binding cannot account for the blue shift of 3nm of heme *a* recorded in the mouse cells at high proton motive force. Furthermore, the shift with calcium is additive to the shift found during both redox titrations and in the fully reduced enzyme, suggesting that the two shifts must originate from a different mechanism. A red shift with a similar difference spectrum to that of calcium was originally observed with pH [26] but this was later attributed to binding of adventitious calcium at low pH when EDTA loses its effectiveness [25]. Here we found that heme *a* of the fully reduced enzyme underwent a blue shift at high pH and that, on fitting the attenuation spectra with the a_{602} and a_{605}, this blue shift could be attributed to a transition from the 605 form to the 602 form with a pK_a of 9.4. These results are different from Vygodina et al. [25] who saw a blue shift at low pH with a pK_a of 5.4 when the oxidase underwent an acidification from pH 8.6. Their shift appeared over a timescale of 3-5 minutes and could not be reversed; we did not measure reversibility due to the difference in methodology but were able to carry out multiple redox titrations suggesting that the shift is reversible. Both studies were carried out in the presence of BAPTA to ensure chelation of adventitious Ca^{2+} at low pH but the buffers, temperature and reducing agents were different.

The F and P_R forms of the BNC have a spectral feature at 607nm [27, 37] that would be similar to the difference between a_{605} and a_{602}. The midpoint potential of these intermediates is very high [38] and they would be reduced to O at a rate kinetically limited either by the transitions themselves (τ≈3ms in the fully reduced enzyme [39]) or electron entry from Cyt*c* in the mixed valence enzyme. Cyt*c* is maintained in close equilibrium with Cu_A during turnover of the isolated enzyme [40], such that the forward flux must be much higher than the net flux (turnover rate). When an individual CytOx reacts with oxygen to form the F state in our titrations, it would be able to rapidly draw electrons from the Cyt*c* pool and re-equilibrate. As the re-equilibration time is much shorter than the turnover time, then the probability of finding an individual CytOx with the BNC in the F or P states would be vanishing small; no evidence of the 607nm feature, or the 580nm feature associated with P form of the BNC has been observed during turnover of the isolated enzyme [40]. An exception to this would be when Cyt*c* is highly oxidized so that the forward flux drops to low levels slowing the rate of re-equilibration. We do observe a weak spectral feature at low pH during oxidizing titrations when Cyt*c* is >99% oxidized (fig. S.4 of the supplementary information) but it has a spectrum very similar to reduced heme a_3. However, this occurs outside the range of the titrations (Cyt*c* 2-98% oxidized) where the a_{602} component is observed. Although the concentration of Cyt*c* is only 70nM in the cell titrations, the cells only occupy 1% (V/V) of the suspension and, if it is assumed the intermembrane space only occupies 1% of the cell, then the concentration of Cyt*c* in the intermembrane space is expected to be ≈ 700μM. This is much higher than in the isolated studies (4μM) and would maintain a high forward flux and fast re-equilibration times to much higher oxidation states. Finally, the a_{602} spectral component is necessary to account for the observed spectral changes even in the reducing (FIRE) titrations which are carried out under anoxic conditions.

The mechanism that generates the spectral shift from 605 to 602nm in heme *a* is not known but it cannot simply be dependent on the oxidation state of heme a_3 because both the a_{605} and the a_{602} states have heme a_3 oxidized. Likewise both azide and cyanide stabilize heme a_3 in the oxidized state but azide stabilizes the 602nm form of heme *a* (fig. 7) and cyanide stabilizes the 605nm form [32]. The shift is not caused by uptake of a proton, but it could possibly be due to some interaction with the oxidation state of Cu_A or Cu_B, or some internal reorganization of the protein such as a conformational change, uptake of water or internal movement of a proton.

4.2 Spectral components of the α-band

The data and analysis presented here show that the spectral shifts in the α-band of CytOx (fig. 1 and 2) can be either accounted for with our spectral fitting model containing the classical spectra of heme *a* and a_3 combined with an addition form of heme *a* with a peak at 602nm (fig. 4a), or a spectral fitting model containing the classical spectrum of heme a_3 and two spectra of half the intensity but similar width to the classical spectrum of heme *a* with peaks at 602 and 607nm (fig. 4b). The first spectral model is consistent with a redox model in which the hemes titrate with considerable redox anticooperativity whereas the second spectral model, previously referred to as the 50:50 model [20], is consistent with a redox model in which the two spectral components titrate as n=1 Nernst functions. The two different spectral models can fit the same spectral data equally well due to the linear relationship between the component absorption spectra and the resulting compound attenuation spectra, and rules out using the quality of the fit as a criterion to determine the correct model.

However, the second model cannot be fitted with a single set of basis spectra; indeed the linear combination of a_{605} and a_{602} needed to generate basis spectra which titrate as (n=1) Nernst functions changes as the midpoint potentials change with the pH or ligation of azide. In contrast our model uses a single set of basis spectra to fit all the data. Furthermore, our model not only accounts for the spectral shifts observed during a redox titration but is also reproduces the anti-cooperativity between the hemes observed with numerous other techniques [20], albeit with a more sophisticated redox model which splits the state with only heme *a* reduced into two states with different spectral properties. Furthermore the combination of our spectral and redox models can predict the attenuation spectra collected by Wilson et al. [10, 17] and Hellwig et al. [11] and explain how these spectra could be incorrectly interpreted resulting in n=1 Nernst functions, further confirming the accuracy of our model and the presence of a 602nm form of heme *a*.

Previously when our spectroscopy model was applied to redox titrations in mouse cells [21], we found that the 602nm component titrated as the a_3 state and the 605nm component titrated as the aa_3 state in a 4 state (*o*, *a*, a_3 and aa_3) anti-cooperativity model. As heme *a* has a high midpoint potential in the *a* state and a low midpoint potential in the aa_3 state, we assigned these two components as heme *a* with high and low midpoint potential, respectively. In this paper, we repeat the same studies in the detergent-solubilized bovine enzyme and find similar results. The 602nm component broadly titrates as the *a* state and the 605nm component broadly titrates as the aa_3 state, except that we needed to include an additional with only heme *a* reduced and having the 605nm spectral component to get a good fit to the data (see fig. S.5 of the supplementary information). This additional state also has a high midpoint potential at low pH and so the nomenclature of high and low potential is not warranted. When the original mouse cell data was re-analyzed with a 5-state model (*o*, a_{602}, a_{605}, a_3 and aa_3), the a_{605} state had a midpoint potential of 250±18mV and so it made negligible contribution to the titration. We repeated the titrations in newer cells with the same methodology and found that the CytOx behaved very similarly to bovine enzyme; here the a_{605} state had a much higher E_m of 298mV and so made a considerable contribution to the titration. Furthermore, the midpoint potentials of the mouse cells were similar to those of the bovine enzyme, albeit all about 10mV higher. The reason for the difference in behavior of the 2 cell cultures from the same cell line is currently not known. It could be speculated that the difference is due to post translational changes that are not being controlled for, between the two cultures.

4.3 Proton coupling

During the catalytic cycle, the enzyme has access to a large number of states and passes through many of those states depending on the rate constants connecting the states. During a redox titration, the enzyme has access to the same states as during catalytic turnover but spends most of its time in the lower energy states. A key difference between a titration and catalytic turnover is that the enzyme has time to relax into lower energy states which are kinetically forbidden on the timescale

of catalytic turnover. It is well known that the isolated enzyme can relax into such states where electron transfer to the binuclear centre is much slower than necessary for turnover, and that the relaxed (slow) enzyme can be returned to the active enzyme by reduction and catalytic turnover [41]. These studies were specifically designed to maintain CytOx in the active form. Firstly, titrations were always preceded by catalytic turnover to consume the oxygen and make the cuvette anoxic. Secondly, the titrations in the oxidizing direction had catalytic turnover, albeit at a very slow rate. Thirdly, the titrations were carried out in a few minutes rather than hours to minimize possible relaxation. Indeed the observation that titrations in the oxidizing and reducing direction overlaid (see fig S.1 for the supplementary information) is strong evidence that the titrations were slow enough to maintain equilibrium between Cyt*c* and heme a_3 yet fast enough to prevent the enzyme relaxing into the slow form. Further evidence for the lack of relaxation is that the titrations in the isolated bovine enzyme were very similar to those in the living mouse cells where this relaxation into the slow form is not expected to occur. Our data should thus provide information on the lowest energy (highest midpoint potential) states that the enzyme passes through during catalytic turnover.

Since the redox titration analysis is sensitive to protonation events which are coupled to the redox centers, they can be used to calculate the pK_a of each site and the number of coupled protons that are bound at a particular pH. Two protonation sites were required to fit the data but it is likely that each of these sites is a mixture of atomic sites that can be protonated in a mutually exclusive manner. The reaction of the fully reduced enzyme with oxygen to form the oxidized enzyme takes up ≈1.6 protons in the pH range 7.5-8.0 [7, 42] so that reduction of the oxidized- to the fully reduced-enzyme must take up ≈2.4 protons given the reduction of oxygen requires 4 substrate protons. Of these 2.4 protons, one was assigned to the reduction of Cu_B, one to reduction of heme a_3 and the remaining 0.4 to the reduction of Cu_A [7]. We find that reduction of heme a_3 from the *o*-state is accompanied with a proton in this pH range (fig. 6c). However, only ≈0.6 protons are taken up on reduction of heme a_3 because the *o* state already has ≈0.4 protons bound, which presumably are bound at a different site and ejected to the p-side upon reduction. Surprisingly, subsequent reduction of heme *a* to form the fully reduced enzyme leads to the loss of ≈0.1 protons, which is counter to notion of the electrostatic coupling of electrons and protons [7, 43]. There is evidence in the atomic structure for such an event: the carboxyl of Asp51 moves from a site buried in the membrane in the oxidized crystal structure, where it is in a polar but non-aqueous environment and expected to have a high pK_a, to a site at the surface in the reduced structure where it is in an aqueous environment and expected to have a low pK_a [44]. In addition, infrared spectroscopy also shows deprotonation of a carboxyl on reduction [45-46]. The net result is that reduction of both hemes is coupled to the uptake of only 0.4 protons rather than one. Of the other two protons, one is probably coupled to reduction of Cu_B and the other must either be coupled to Cu_A, Cu_B or both.

The midpoint potentials of the $o \rightarrow a_{605}$ and $o \rightarrow a_3$ redox couples were strongly pH dependent above pH 7.0. At high pH, when the interacting proton has been drawn off, the midpoint potential of these couples is lower than that of heme *a* when heme a_3 is reduced ($a_3 \rightarrow aa_3$ couple). This is contrary to a simple electrostatic model of anti-cooperativity [19], where the hemes inherently have a high midpoint potential which is then lowered when the other heme is reduced, due to the electrostatic repulsion. Instead the data suggests that these couples inherently have a low midpoint potential which is raised by interaction with a proton. The midpoint potential of the $o \rightarrow a_{602}$ couple is remarkably independent of pH above pH 7.0 because the pKa for the first proton binding event is similar to that of the *o* state. This would suggest that heme *a* gains a high potential in this state, and presumably its spectral shift, by a mechanism not dependent on proton uptake.

4.4 Azide

Previous studies examining small changes in the absorption spectrum of the oxidized enzyme in the Soret band upon binding of azide at pH 8.0, found a high affinity site with a K_d of 64μM and a low affinity site with a K_d of 20mM [47]. The high affinity site had a band at 2051cm^{-1} in infrared

spectra [47-48] and the low affinity site at 2041cm^{-1} [48], both consistent with the bound N_3 anion rather than neutral HN_3. The band from the low affinity site splits on isotopic labeling of azide indicating that it is bound to a metal ion whereas the high affinity site does not, suggesting it binds to the protein [48]. Both bands are lost on addition of cyanide [47-48], even though only one cyanide binds per enzyme [48]. The crystal structure of bovine oxidase shows two bound azides, one at the BNC and one on the periphery of subunit 1 approximately 16Å from both hemes where it is hydrogen bonded to Tyr379 and Asn422 [49]. A re-analysis of two-wavelength titration data in terms of the redox anti-cooperativity [50] found that the K_d for binding when heme a_3 was reduced was extremely high, suggesting that azide had the effect of stabilizing the a_{602} state and that reduction of heme a_3 at very low redox potentials required the ejection of azide [50]. We were able to study the binding of azide with more detail and resolved two binding events. The disassociation constants for binding to the oxidized state were consistent with those measured from the changes in the absorption spectrum [47]. The K_d for binding of azide to the a_{602} state for the low and high affinity sites were similar to those of the *o* state but the K_d of binding to the a_{605}, a_3 and aa_3 states was considerably increased for the high affinity site and increased to such an extent for the low affinity site that it could not be resolved. The overall result was that the midpoint potential of the a_{602} state was independent of azide whereas the midpoint potential of the $o \rightarrow a_{605}$, $o \rightarrow a_3$ and $a \rightarrow aa_3$ couples rapidly decreased with azide concentration. These changes on binding of azide suggest that the resulting blue shift is not a direct effect of the azide on heme *a* but rather it is stabilizing the a_{602} form of heme *a* that is already present in the unligated enzyme. The a_{602} form was also found to be stabilized in the living cells on addition of azide further confirming that we are able to make precise measurements of CytOx in this system. The effect of azide binding to the high affinity site on the midpoint potential of the $o \rightarrow a_{605}$ and $o \rightarrow a_3$ couples is similar to the removal of the interacting proton, suggesting that azide possibly stabilizes the structure with this site unprotonated.

The dependence of K_d on reduction state is consistent with the low affinity site being at the BNC as the negative charge would lower the midpoint potential of heme a_3 and, to lesser extent, heme *a* as it is further away. The same argument could be made for the high affinity site: it also involves binding at the BNC rather than at the peripheral site in the crystal structure, although steric hindrance would preclude two azides in the BNC. If azide does bind with high affinity to the peripheral site then there must be some anti-cooperative mechanism to eject this azide from this site when cyanide binds at the BNC [49]. A recent femtosecond x-ray crystallography study has shown that, on disassociation of CO from heme a_3, there is a distortion of the porphyrin ring and movement of Val380, which contacts with the face of the C pyrrole ring. This movement leads to the partial unwinding of helix X at residues 380-384 [51] which runs between heme *a* and a_3 and contains their axial ligands His378 and His376, respectively. Helix X also contains Ser382 which H-bonds to the hydroxyl at the top of the farnesyl side chain of heme *a* in the oxidized enzyme but not the reduced enzyme [44], and Tyr379 that H-bonds to the azide bound at the peripheral site [49]. This conformational change could be the anti-cooperative coupling between the binding of cyanide to heme a_3 and binding of azide at the peripheral site, as the crystal structure of the former is in the wound conformation and the latter in the unwound conformation [51].

5. Conclusion

This work confirms and extends our previous work in mouse cells. We show conclusively that there are two spectral forms of heme *a*: the classic form with a peak at 605nm and a second form with a peak at 602nm. Our titrations in the azide-ligated enzyme were, for the first time, able to resolve the two azide binding sites and suggest that binding at the peripheral site of the crystal structure is also able to stabilize the 602nm form of heme *a*. We have extended the standard 4-state redox anticooperativity model to include two states in which only heme *a* is reduced but has either the 602 or 605nm form, and shown that the pH-dependence of the midpoint potentials of these two states is very different. This 5-state model reproduces the anticooperativity between the hemes of a standard 4-state model and can, for the first time, rigorously account for the spectral shifts seen during redox

titrations. Using these spectral components to analyze the spectra from CytOx after CO photolysis in the mixed valence enzyme [12] or after photo injection of an electron in the Cu_A site [8] would likely provide information as to the conditions that generate this blue shift. Finally, this work also confirms that we are able to successfully perform redox titrations in living cells and accurately determine the heme midpoint potentials. The advantage of working in the living cell is that the CytOx is in its authentic environment, is pumping protons against the proton motive force (which can be quantified [52]), and is subject to post translational changes [53].

Acknowledgements

Roger Springett is grateful to Jiapeng Zhu and Judy Hirst at the Mitochondrial Biology Unit for use of the protein.

This work was funded by European Community's 7th Framework Program under grant agreement FP7-PEOPLE-2013-IIF No. 628575.

References

[1] I. Belevich, M.I. Verkhovsky, Molecular mechanism of proton translocation by cytochrome c oxidase, Antioxid Redox Signal, 10 (2008) 1-29.

[2] S. Iwata, C. Ostermeier, B. Ludwig, H. Michel, Structure at 2.8 A resolution of cytochrome c oxidase from Paracoccus denitrificans, Nature, 376 (1995) 660-669.

[3] S. Shimada, K. Shinzawa-Itoh, J. Baba, S. Aoe, A. Shimada, E. Yamashita, J. Kang, M. Tateno, S. Yoshikawa, T. Tsukihara, Complex structure of cytochrome c-cytochrome c oxidase reveals a novel protein-protein interaction mode, EMBO J, 36 (2017) 291-300.

[4] P.R. Rich, Mitochondrial cytochrome c oxidase: catalysis, coupling and controversies, Biochem Soc Trans, 45 (2017) 813-829.

[5] M. Fabian, W.W. Wong, R.B. Gennis, G. Palmer, Mass spectrometric determination of dioxygen bond splitting in the "peroxy" intermediate of cytochrome c oxidase, Proc Natl Acad Sci U S A, 96 (1999) 13114-13117.

[6] G.T. Babcock, M. Wikstrom, Oxygen activation and the conservation of energy in cell respiration, Nature, 356 (1992) 301-309.

[7] R. Mitchell, P.R. Rich, Proton uptake by cytochrome c oxidase on reduction and on ligand binding, Biochim Biophys Acta, 1186 (1994) 19-26.

[8] I. Belevich, D.A. Bloch, N. Belevich, M. Wikstrom, M.I. Verkhovsky, Exploring the proton pump mechanism of cytochrome c oxidase in real time, Proc Natl Acad Sci U S A, 104 (2007) 2685-2690.

[9] D.F. Wilson, J.G. Lindsay, E.S. Brocklehurst, Heme-heme interaction in cytochrome oxidase, Biochim Biophys Acta, 256 (1972) 277-286.

[10] J.G. Lindsay, D.F. Wilson, Apparent adenosine triphosphate induced ligand change in cytochrome a 3 of pigeon heart mitochondria, Biochemistry, 11 (1972) 4613-4621.

[11] P. Hellwig, S. Grzybek, J. Behr, B. Ludwig, H. Michel, W. Mantele, Electrochemical and ultraviolet/visible/infrared spectroscopic analysis of heme a and a3 redox reactions in the cytochrome c oxidase from Paracoccus denitrificans: separation of heme a and a3 contributions and assignment of vibrational modes, Biochemistry, 38 (1999) 1685-1694.

[12] M.I. Verkhovsky, A. Jasaitis, M. Wikstrom, Ultrafast haem-haem electron transfer in cytochrome c oxidase, Biochim Biophys Acta, 1506 (2001) 143-146.

[13] L.E. Andreasson, Characterization of the reaction between ferrocytochrome c and cytochrome c oxidase, Eur J Biochem, 53 (1975) 591-597.

[14] G.L. Liao, G. Palmer, The reduced minus oxidized difference spectra of cytochromes a and a3, Biochim Biophys Acta, 1274 (1996) 109-111.

[15] A. Tzagoloff, D.C. Wharton, Studies on the Electron Transfer System. Lxii. The Reaction of Cytochrome Oxidase with Carbon Monoxide, J Biol Chem, 240 (1965) 2628-2633.

[16] D.F. Blair, D.F. Bocian, G.T. Babcock, S.I. Chan, Evidence for modulation of the heme absorptions of cytochrome c oxidase by metal-metal interactions, Biochemistry, 21 (1982) 6928-6935.

[17] P.L. Dutton, D.F. Wilson, C.P. Lee, Oxidation-reduction potentials of cytochromes in mitochondria, Biochemistry, 9 (1970) 5077-5082.

[18] P. Nicholls, L.C. Petersen, Haem-haem interactions in cytochrome aa3 during the anaerobic-aerobic transition, Biochim Biophys Acta, 357 (1974) 462-467.

[19] L.I. Krishtalik, The negative cooperativity in cytochrome c oxidase redox reactions: the electrostatic effect, Arch Biochem Biophys, 243 (1985) 701-702.

[20] M.K.F. Wikstrom, H.J. Harmon, W.J. Ingledew, B. Chance, A re-evaluation of the spectral, potentiometric and energy-linked properties of cytochrome c oxidase in mitochondria, FEBS Lett, 65 (1976) 259-277.

[21] N. Kim, M.O. Ripple, R. Springett, Spectral components of the alpha-band of cytochrome oxidase, Biochim Biophys Acta, 1807 (2011) 779-787.

[22] M. Wikstrom, H. Saari, A spectral shift in cytochrome a induced by calcium ions, Biochim Biophys Acta, 408 (1975) 170-179.

[23] A. Kirichenko, T. Vygodina, H.M. Mkrtchyan, A. Konstantinov, Specific cation binding site in mammalian cytochrome oxidase, FEBS Lett, 423 (1998) 329-333.

[24] A.V. Kirichenko, U. Pfitzner, B. Ludwig, C.M. Soares, T.V. Vygodina, A.A. Konstantinov, Cytochrome c oxidase as a calcium binding protein. Studies on the role of a conserved aspartate in helices XI-XII cytoplasmic loop in cation binding, Biochemistry, 44 (2005) 12391-12401.

[25] T.V. Vygodina, A. Kirichenko, A.A. Konstantinov, Cation Binding Site of cytochrome c oxidase: Progress report, Biochim Biophys Acta, (2014).

[26] H. Saari, T. Penttila, M. Wikstrom, Interactions of Ca2+ and H+ with heme A in cytochrome oxidase, J Bioenerg Biomembr, 12 (1980) 325-338.

[27] M. Fabian, G. Palmer, Proton involvement in the transition from the "peroxy" to the ferryl intermediate of cytochrome c oxidase, Biochemistry, 40 (2001) 1867-1874.

[28] A.L. Smith, [13] Preparation, properties, and conditions for assay of mitochondria: Slaughterhouse material, small-scale, Methods in Enzymology, 10 (1967) 81-86.

[29] J.E. Walker, J. Mark Skehel, S.K. Buchanan, [2] Structural analysis of NADH: Ubiquinone oxidoreductase from bovine heart mitochondria, Methods in Enzymology, 260 (1995) 14-34.

[30] H. Qian, Open-system nonequilibrium steady state: statistical thermodynamics, fluctuations, and chemical oscillations, J Phys Chem B, 110 (2006) 15063-15074.

[31] J.H. Prinz, H. Wu, M. Sarich, B. Keller, M. Senne, M. Held, J.D. Chodera, C. Schutte, F. Noe, Markov models of molecular kinetics: generation and validation, J Chem Phys, 134 (2011) 174105.

[32] A.J. Moody, P.R. Rich, The effect of pH on redox titrations of haem a in cyanide-liganded cytochrome-c oxidase: experimental and modelling studies, Biochim Biophys Acta, 1015 (1990) 205-215.

[33] N. Kojima, G. Palmer, Further characterization of the potentiometric behavior of cytochrome oxidase. Cytochrome alpha stays low spin during oxidation and reduction, J Biol Chem, 258 (1983) 14908-14913.

[34] D.W. Marquardt, An Algorithm for Least-Squares Estimation of Nonlinear Parameters, Journal of the Society for Industrial and Applied Mathematics, 11 (1963) 431-441.

[35] P. Nicholls, H.K. Kimelberg, Cytochromes a and a3. Catalytic activity and spectral shifts in situ and in solution, Biochim Biophys Acta, 162 (1968) 11-21.

[36] A.V. Dyuba, T.V. Vygodina, A.A. Konstantinov, Reconstruction of absolute absorption spectrum of reduced heme a in cytochrome C oxidase from bovine heart, Biochemistry (Mosc), 78 (2013) 1358-1365.

[37] M. Wikstrom, Energy-dependent reversal of the cytochrome oxidase reaction, Proc Natl Acad Sci U S A, 78 (1981) 4051-4054.

[38] M. Wikstrom, J.E. Morgan, The dioxygen cycle. Spectral, kinetic, and thermodynamic characteristics of ferryl and peroxy intermediates observed by reversal of the cytochrome oxidase reaction, J Biol Chem, 267 (1992) 10266-10273.

[39] K. Faxen, G. Gilderson, P. Adelroth, P. Brzezinski, A mechanistic principle for proton pumping by cytochrome c oxidase, Nature, 437 (2005) 286-289.

[40] M.G. Mason, P. Nicholls, C.E. Cooper, The steady-state mechanism of cytochrome c oxidase: redox interactions between metal centres, Biochem J, 422 (2009) 237-246.

[41] D. Jancura, V. Berka, M. Antalik, J. Bagelova, R.B. Gennis, G. Palmer, M. Fabian, Spectral and kinetic equivalence of oxidized cytochrome C oxidase as isolated and "activated" by reoxidation, J Biol Chem, 281 (2006) 30319-30325.

[42] S. Hallen, T. Nilsson, Proton transfer during the reaction between fully reduced cytochrome c oxidase and dioxygen: pH and deuterium isotope effects, Biochemistry, 31 (1992) 11853-11859.

[43] P.R. Rich, B. Meunier, R. Mitchell, A. Moody, P. Mitchell, Coupling of charge and proton movement in cytochrome c oxidase, Biochim Biophys Acta, 1275 (1986) 91-95.

[44] T. Tsukihara, K. Shimokata, Y. Katayama, H. Shimada, K. Muramoto, H. Aoyama, M. Mochizuki, K. Shinzawa-Itoh, E. Yamashita, M. Yao, Y. Ishimura, S. Yoshikawa, The low-spin heme of cytochrome c oxidase as the driving element of the proton-pumping process, Proc Natl Acad Sci U S A, 100 (2003) 15304-15309.

[45] P. Hellwig, T. Soulimane, G. Buse, W. Mantele, Similarities and dissimilarities in the structure-function relation between the cytochrome c oxidase from bovine heart and from Paracoccus denitrificans as revealed by FT-IR difference spectroscopy, FEBS Lett, 458 (1999) 83-86.

[46] D. Okuno, T. Iwase, K. Shinzawa-Itoh, S. Yoshikawa, T. Kitagawa, FTIR detection of protonation/deprotonation of key carboxyl side chains caused by redox change of the Cu(A)-heme a moiety and ligand dissociation from the heme a3-Cu(B) center of bovine heart cytochrome c oxidase, J Am Chem Soc, 125 (2003) 7209-7218.

[47] W. Li, G. Palmer, Spectroscopic characterization of the interaction of azide and thiocyanate with the binuclear center of cytochrome oxidase: evidence for multiple ligand sites, Biochemistry, 32 (1993) 1833-1843.

[48] S. Yoshikawa, W.S. Caughey, Infrared evidence of azide binding to iron, copper, and non-metal sites in heart cytochrome c oxidase, J Biol Chem, 267 (1992) 9757-9766.

[49] M.J. Fei, E. Yamashita, N. Inoue, M. Yao, H. Yamaguchi, T. Tsukihara, K. Shinzawa-Itoh, R. Nakashima, S. Yoshikawa, X-ray structure of azide-bound fully oxidized cytochrome c oxidase from bovine heart at 2.9 A resolution, Acta Crystallogr D Biol Crystallogr, 56 (2000) 529-535.

[50] M. Wikstrom, K. Krab, M. Saraste, Cyochrome Oxidase: A synthesis, Academic Press, London, 1981.

[51] I. Ishigami, N.A. Zatsepin, M. Hikita, C.E. Conrad, G. Nelson, J.D. Coe, S. Basu, T.D. Grant, M.H. Seaberg, R.G. Sierra, M.S. Hunter, P. Fromme, R. Fromme, S.R. Yeh, D.L. Rousseau, Crystal structure of CO-bound cytochrome c oxidase determined by serial femtosecond X-ray crystallography at room temperature, Proc Natl Acad Sci U S A, 114 (2017) 8011-8016.

[52] N. Kim, M.O. Ripple, R. Springett, Measurement of the Mitochondrial Membrane Potential and pH Gradient from the Redox Poise of the Hemes of the bc1 Complex., Biophys J, 102 (2012) 1194-1203.

[53] I. Lee, A.R. Salomon, S. Ficarro, I. Mathes, F. Lottspeich, L.I. Grossman, M. Huttemann, cAMP-dependent tyrosine phosphorylation of subunit I inhibits cytochrome c oxidase activity, J Biol Chem, 280 (2005) 6094-6100.

Figure Legends

Figure 1. Changes in the α-band attenuation spectrum of CytOx on reduction from the oxidized state at pH 8.0. The Grey vertical line is drawn at 605nm to emphasize the small spectral shift. The inset shows the spectrum at a redox potential of 280mV minus the fully oxidized spectrum (red) and the fully reduced spectrum minus the spectrum at 280mV (blue).

Figure 2. Wavelength shift of the α-band of heme *a* as a function of redox potential at increasing pHs (7.0, 7.5, 8.0, 8.5 and 9.0). Blue and red traces indicate the absence of calcium (chelated by 200μM BAPTA) and presence of calcium (addition of 250μM $CaSO_4$), respectively. Inset: wavelength shift when fully reduced. Green bars are the shift on calcium binding to the fully reduced enzyme.

Figure 3. The fraction of the a_{605} and a_{602} spectra to the attenuation spectrum of fully reduced CytOx as a function of pH. CytOx was reduced with NADH, using PES as a redox mediator, and in the presence of 200μM BAPTA to chelate calcium. Data points are from 3 studies and the lines are from a disassociation function with a pK_a of 9.4.

Figure 4. Redox titrations of the α-band of CytOx at pH 7.5. The experimental data is shown as points, the lines are a fit to a redox model and the spectra for the fitting model are shown in the insert. a) Titrations from the α-band using the standard a_{605} and a_3 spectra along with the a_{602} spectrum. The data was fit to a 5 state model of redox cooperativity. b) The same spectra data as a) but fitted using a linear combination of the a_{605} and a_{602} spectra which titrate as n=1 Nernst functions (lines). c) Titrations from the Soret-band using the reference spectrum of heme *a* (a_{446}) and a_3, and the reference spectrum of heme *a* blue shifted by 3nm (a_{443}). The lines are from the model in a) shown to emphasize the differences between the data obtained from the α- and Soret-bands.

Figure 5. Redox titrations of the α-band of CytOx at increasing pH (6.0 to 9.0). The experimental data is displayed as points and the lines are a fit to a 15-state (o, a602, a605, a3 and aa3 with 0, 1 or 2 bound protons) model with the standard energies fitted simultaneously to all the data points.

Figure 6. pH dependence of a) the standard energies, b) midpoint potentials and c) number of bound protons of the 15-state model fitted to the data of fig. 5. The data points in b) are the midpoint potentials of a 5 state model fitted individually to the data at each pH.

Figure 7. Redox titrations of the α-band of CytOx at increasing concentrations of sodium azide (pH 8.0). The points are the data and the lines are from a simultaneous fit to a redox model which consisted of unligated and singly ligated *o*, a_{602}, a_{605}, a_3 and aa_3, and doubly ligated *o* and a_{602}.

Figure 8. Effective midpoint potentials in the presence of azide. The solid lines are the predicted midpoint potentials from the redox model with both binding sites and the dotted lines are the midpoint potentials for only the high affinity site. The triangles are the midpoint potentials of a 5 state model fitted individually to the data at each pH. The circles are the midpoint potentials from the mouse cells.

Figure 9. Redox titrations of the α-band of CytOx from living RAW 264.7 macrophages in the absence and presence of 1mM of sodium azide.

Tables

State	E_0 ($0H^+$)	E_0 ($1H^+$)	E_0 ($2H^+$)	pK_a 0→1	pK_a 1→2
O	0	-33.2±7.8	68.8±18.6	7.54±0.13	5.34±0.43
a602	-317.5±1.1	-344.6±4.3	-297.1±4.7	7.44±0.09	6.23±0.03
a605	-235.9±16.5	-349.0±4.4	-275.6±4.4	8.84±0.34	5.81±0.11
a3	-236.4±8.6	-370.3±4.8	-286.1±9.9	9.18±0.07	5.63±0.08
aa3	-510.2±2.6	-596.0±3.7	-536.1±6.4	8.39±0.10	6.03±0.05

Table 1 Standard energies for unprotonated, singly protonated and double protonated states, and pK_as for the model of fig. 4. Values are expressed as mean±SD (n=3 sets of titrations with each set having 7 pHs

E_m	+FCCP	−Azide	+Azide
o→a_{602}	329.9±4.3	325.4±3.0	333.3±2.4
o→a_{605}	251.2±19	297.6 ±2.2	<230
o→a_3	292.9±2.9	315.7±7.3	283.0±6.1
a_3→aa_3	223.9±7.9	243.9±3.2	243.3±5.9

Table 2. Midpoint potentials (E_m) for a 5 state redox model to redox titrations carried out in RAW 264.7 mouse macrophages in the presence or absence of 1mM azide. +FCCP reanalysis of the FCCP treated data from [21] in the absence of azide. Values are presented as mean±SD (n=6, 4 and 4, respectively)

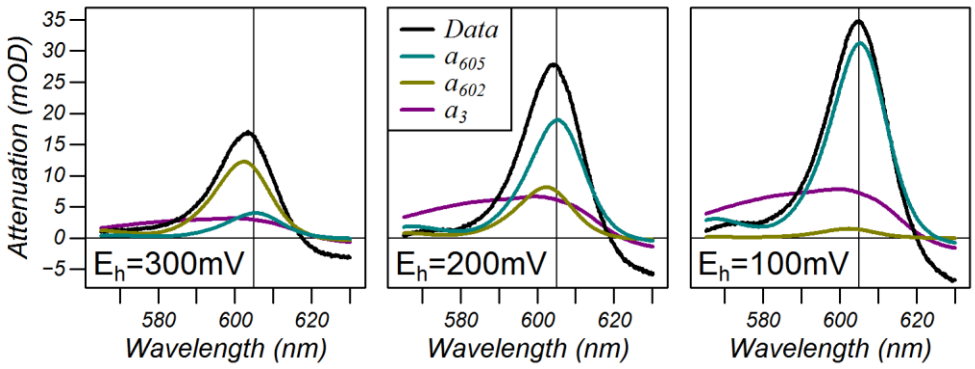

Graphical abstract